Differential impact of self and environmental antigens on the ontogeny and maintenance of $CD4^+$ T cell memory

Thea Hogan[1†], Maria Nowicka[2†], Daniel Cownden[3], Claire Pearson[4], Andrew J. Yates[2*] and Benedict Seddon[1*]

[1]Institute of Immunity and Transplantation, Division of Infection and Immunity, UCL, Royal Free Hospital, Rowland Hill Street, London NW3 2PF, United Kingdom
[2]Department of Pathology and Cell Biology, Columbia University Medical Center, 701 West 168th Street, New York, NY 10032, USA
[3]Institute of Infection, Immunity and Inflammation, University of Glasgow, Glasgow G3 8TA, United Kingdom
[4]Kennedy Institute of Rheumatology, University of Oxford, Roosevelt Drive, Headington, Oxford OX3 7FY, United Kingdom

† Contributed equally
* Contributed equally; address correspondence to either author
andrew.yates@columbia.edu, benedict.seddon@ucl.ac.uk

Abstract

Laboratory mice not exposed to overt infections nevertheless develop populations of circulating memory phenotype (MP) $CD4^+$ T cells, presumably in response to environmental, commensal or self-antigens. The relative importance and timing of the forces that generate these populations remain unclear. Here we combine mathematical models with data from studies tracking the generation of $CD4^+$ MP T cell subsets in mice of different ages, housed in facilities that differ in their 'dirtiness'. We find evidence for a developmental pathway from naive $CD4^+$ to central MP to effector MP cell populations, and infer that both memory subsets are heterogeneous in their rates of turnover. We also infer that early exposure to self and environmental antigens establishes persistent populations of both MP subsets at levels determined largely, but not exclusively, by the dirtiness of the environment. After the first few weeks of life, however, these populations are continuously supplemented by new memory cells at rates that appear to be independent of environment, likely in response to self or ubiquitous commensal antigens.

Introduction

Conventional memory T cells are defined as lymphocytes which respond rapidly upon re-encounter with previously-encountered epitopes (Gourley *et al.*, 2004, Kaech and Wherry, 2007). In mice, memory T cells exhibit considerable heterogeneity in their function, circulation patterns, response to re-challenge, and capacities for proliferative self-renewal and survival (Farber, 2000, Gossel *et al.*, 2017, Jameson and Masopust, 2009, Kaech and Wherry, 2007). This phenotypic heterogeneity is reflected in differential expression of various cell-surface molecules. In uninfected naive mice, there are at least two distinct populations of recirculating cells distinguished by their expression of the lymph node homing receptor L-selectin (CD62L); $CD44^{hi}$ $CD62L^-$ effector memory (T_{EM}) and $CD44^{hi}$ $CD62L^+$ central memory (T_{CM}) cells. During immune responses to active infection, there is an even more complex mix of effector and memory intermediates (Jameson and Masopust, 2018).

While it is clear that memory to infection resides amongst these $CD44^{hi}$ subsets, it is also evident that they are generated in naive mice in the absence of overt infection. Their functional significance is not fully understood, but there is evidence they can augment primary immune responses. These memory-phenotype (MP) $CD4^+$ T cells can facilitate rapid production of IFN-γ during the early inflammatory phase of the immune response

to *Toxoplasma gondii* infection and enhance T_H1-type CD4+ T cell responses later in infection (Kawabe *et al.*, 2017). There is also evidence that MP cells are capable of making rapid cross-reactive responses during primary infections (Min and Paul, 2005). Given that such MP cells represent the majority of the memory compartment in specific pathogen-free (SPF) mice (Kawabe *et al.*, 2017), a better understanding of how these cells are generated and maintained is crucial to better understand their function and impact upon conventional memory to defined challenges.

The precise nature of the forces driving the generation of MP cells remains unclear. Their development does appear to be dependent upon a TCR-mediated activation event. Evidence for this comes from observations that $CD28^{-/-}$ mice have greatly reduced numbers of MP populations (Kotani *et al.*, 2006), while mice lacking canonical NF-κB signalling, an obligate pathway in T cell activation, are completely devoid of such cells (Webb *et al.*, 2019). Whether the stimuli for these activation triggers derive from self or foreign recognition events is unknown. Their generation may reflect a stochastic process in which naive CD4 T cells occasionally encounter homeostatic stimuli that are above an activation threshold (Sprent and Surh, 2011), and indeed MP cells are generated not only in lymphopenia but also constitutively under replete conditions throughout life (Gossel *et al.*, 2017, Kawabe *et al.*, 2017). There is a positive correlation between the affinity of naive $CD4^+$ T cells to self-antigens and the potential for differentiating into MP cells (Kawabe *et al.*, 2017), although self-reactivity is also positively correlated to reactivity to foreign antigens (Mandl *et al.*, 2013). Stronger evidence supporting an autoreactive stimulus comes from the failure of broad-spectrum antibiotics to prevent conversion of naive cells to MP cells following adoptive transfer in vivo, and the observation that mice raised in germ free conditions contain similar numbers of MP cells as those in SPF conditions (Kawabe *et al.*, 2017). However, there is also a role for foreign environmental antigen in generating T cell memory compartments, since mice raised in more antigenically diverse environments, but still in the absence of overt infection, exhibit larger peripheral memory $CD8^+$ T cell pools than SPF mice (Beura *et al.*, 2016). When exactly such environmental stimuli impact upon memory compartment development, or how foreign and self reactivity combine to form the memory compartments, is unknown.

The differentiation pathways of these MP cells are also poorly understood. They may derive either directly from the naive T cell pool or through interconversion of other memory phenotypes. Amongst CD8 cells, there is evidence that some MP subpopulations are generated in the thymus (Lee *et al.*, 2011). In the case of CD4 lineage cells, it has been suggested that MP $CD4^+$ T cells derive from peripheral naive phenotype cells in a thymus-independent fashion (Kawabe *et al.*, 2017). While both CD4 T_{EM} and CD4 T_{CM} are produced constitutively in adult mice (Gossel *et al.*, 2017), it remains unclear how their differentiation patterns relate to those of classically antigen-stimulated naive T cells.

In this study we aimed to characterise the development and maintenance of memory CD4 T cell subsets in adult mice to identify the nature and timing of the signals driving these dynamics in the absence of overt infection. To do this we quantified the homeostasis and ontogeny of memory CD4 T cells in identical strains of mice raised in two different animal facilities with distinct caging environments; those housed in individually ventilated cages (IVCs) and fed irradiated water, and those fed untreated tap water and housed in open cages, who might consequently be exposed to a greater variety of environmental antigens. We made use of an established temporal fate-mapping model in both cohorts, which allowed us to track the development of T cells under replete conditions (Gossel *et al.*, 2017, Hogan *et al.*, 2015a). We also used data from germ-free (GF) mice to dissect further the relative contributions of self and environmental antigens to the generation and maintenance of MP cells.

Results

Modelling the ontogeny and homeostasis of CD4$^+$ MP T cell subsets

We employed a system described previously (Gossel *et al.*, 2017, Hogan *et al.*, 2015a) to examine the flow of cells into memory subsets (Fig. 1A). Briefly, CD45.1$^+$ C57Bl6/SJL host mice of various ages were treated with optimised doses of the transplant conditioning drug busulfan to selectively deplete haematopoeitic stem cells (HSC). The HSC compartment was then reconstituted by bone marrow transplantation (BMT) with congenically labelled bone marrow from CD45.2$^+$ C57Bl6/J donors. The progeny of donor HSC were then followed as they developed in the thymus and percolated into the peripheral T cell pools, initially replete with host-derived cells. Total numbers of CD4$^+$ naive T cells and T_{CM} and T_{EM} cells in these busulfan chimeric mice were normal, in comparison to untreated WT controls (Fig. S1), confirming that the busulfan treatment regime left peripheral compartments intact (Gossel *et al.*, 2017, Hogan *et al.*, 2015a). The kinetics with which donor-derived cells infiltrate the peripheral compartments – first naive, and then memory subsets – are rich in information regarding developmental pathways, rates of turnover and differentiation of lymphocyte populations, and any heterogeneity in homeostatic dynamics within them (Gossel *et al.*, 2017, Hogan *et al.*, 2015a, Rane *et al.*, 2018).

We studied busulfan chimeric mice from two housing facilities that employed different levels of mouse containment. At the MRC National Institute for Medical Research (NIMR), mice were held in open cages and fed untreated tap water, while mice held at the UCL Comparative Biology Unit (UCL) were maintained in individually ventilated cages (IVCs) and fed irradiated water. Henceforth we refer to UCL sourced mice as 'clean' and NIMR sourced mice as 'dirty', in reference to the presumed difference in health status of the mice. We use these terms for clarity, but emphasise that they are relative; mice co-housed with pet-store or feral mice would be expected to be substantially 'dirtier' (Beura *et al.*, 2016), and those in turn are cleaner than truly feral mice. In both environments, the same C57Bl6/SJL strain was analysed by the same researcher and cells were enumerated using the same single CASY counter. In mice aged 10 weeks and older, the numbers of naive CD4 T cells in mice from clean and dirty environments were broadly similar (Fig. 1B, left panel). The total sizes (host+donor) of all circulating memory CD4 T cell subsets remained relatively stable over the time frame of analysis, but were already significantly larger in dirty mice (Fig. 1B, right panels) at age 10 weeks. Following BMT, donor-derived memory T cells accumulated in similar numbers in the two environments (Fig. 1C). Therefore, these two observations result in a lower proportional replacement of pre-existing memory cells with donor memory cells in dirty mice (Fig. 1D).

To quantify the cellular processes underlying these kinetics, we first considered a simple mechanistic explanation shown schematically in Fig. 2A. In this model, each memory population (CD4 T_{CM} or T_{EM}) is fed at a constant *per capita* rate from a precursor population (source). We refer to this rate as the force of recruitment, φ. The total cellular flux into memory per day is then φ multiplied by the size of the source population, which in principle could be naive CD4 T cells, or the complementary memory population. We assume that memory cells are then lost at a constant net *per capita* rate λ which is the balance of loss (turnover) and proliferative self-renewal. In particular, the 'clonal half-life' $\ln(2)/\lambda$ is the average time taken for a self-renewing population to halve in size and may be much longer than the lifespan of any particular cell within it.

We also considered a 'two phase' model of memory dynamics, illustrated in Fig. 2B, which was motivated by three observations. First, donor CD4 T_{CM} and T_{EM} in busulfan chimeras express Ki67, a marker of recent cell division, at higher levels than host cells for some time after BMT (Gossel *et al.*, 2017), although these levels eventually converge (data not shown). These observations suggest that the simplest model may not fully capture memory T cell dynamics. Second, we previously found evidence, using BrdU labelling in WT mice, that both CD4 T_{EM} and T_{CM} appear to be kinetically heterogeneous, with at least two subpopulations turning over and dividing at different rates (Gossel *et al.*, 2017). Third, and consistent with this picture, the increases in donor chimerism that we observed in both T_{CM} and T_{EM} with time post-BMT were suggestive of a biphasic kinetic, with a relatively

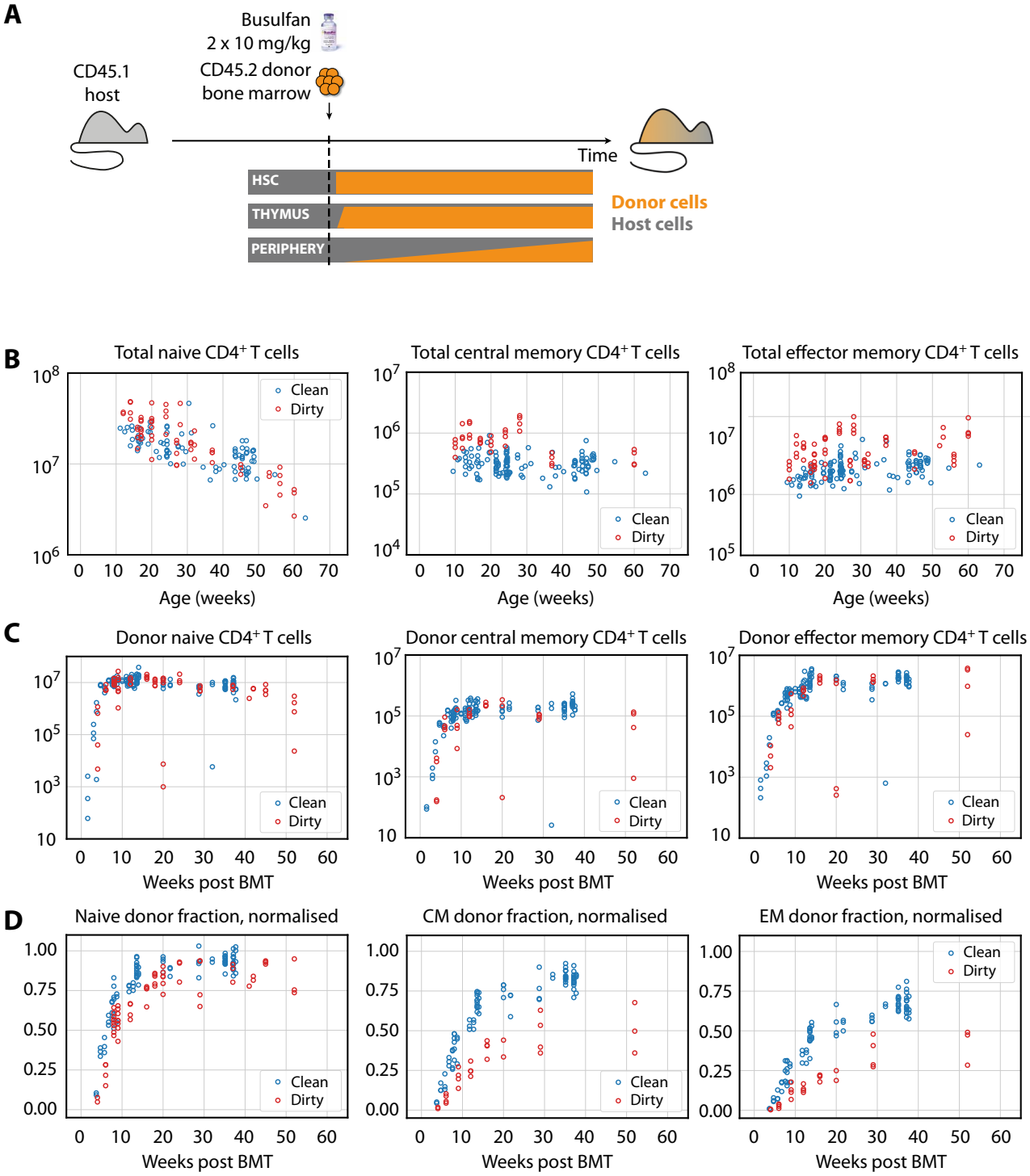

Figure 1: **(A)** Generating bone marrow chimeras to map T cell homeostasis. Donor T cells (orange) differentiate and percolate through the thymus and periphery, replacing host cells (grey). **(B)** Comparing total numbers of $CD4^+$ naive, T_{CM} and T_{EM} cells in clean and dirty chimeric mice. **(C)** Numbers of donor-derived $CD4^+$ subsets recovered from spleen and lymph nodes of clean and dirty chimeric mice. Bone marrow transplants (BMT) were performed in mice between ages 5-26 weeks. **(D)** The donor fraction (chimerism) within $CD4^+$ T cell subsets, varying with time post BMT, normalised to the chimerism in the double-positive thymocytes in each mouse.

rapid accumulation of donor cells followed by a slower increase (Fig. 1D). As shown in Methods and Materials, the rate of accumulation of a donor memory subset is dictated by both the dynamics of influx and its net loss rate, λ. Therefore, all three observations are consistent with a mechanism in which cells newly recruited into memory comprise a subpopulation that both divides rapidly and has a high net loss rate λ_{fast}. These cells then transition to a more quiescent state that divides more slowly and also has a lower net loss rate, $\lambda_{\text{slow}} < \lambda_{\text{fast}}$ (Fig. 2B). The transient differences in Ki67 expression in donor and host memory cells could then be explained by an enrichment for 'new' memory (donor cells) in the fast phase in the weeks immediately following BMT, and not by any intrinsic differences in the behaviour of donor and host cells. Further, this transient difference in Ki67 expression implies a linear flow from fast to slow, rather than a branched process of establishment of the two populations separately; in the latter case, we would expect no differences in Ki67 expression between host and donor cells at any time.

While the two-phase model is perhaps a minimal description of these observations, it seems plausible that any transition from active to quiescent memory might involve more stages or indeed be continuous. We previously found evidence for smooth changes in the rates of division and/or loss of naive T cells with their post-thymic age (Rane *et al.*, 2018). We therefore also considered a model in which the net loss rate of a cohort of cells λ changes continuously with the time since their common ancestor entered the memory compartment, a (the 'age-dependent loss model', Fig. 2C). While the observations above are most consistent with $\lambda_{\text{slow}} < \lambda_{\text{fast}}$, or a decreasing $\lambda(a)$, when fitting the two-phase and age-dependent loss models we placed no constraints on these parameters and allowed the data to determine their values. For the age-dependent loss model we explored a variety of forms for $\lambda(a)$ (see Methods and Materials).

Finally, we considered an alternative form of heterogeneity in memory, in which subpopulations of CD4 T_{CM} and T_{EM} generated early in life resist displacement by newer cells (Gossel *et al.* (2017); Fig. 2D). These 'incumbent memory' populations, assumed to be stable in numbers and entirely host-derived (that is, established before 5 weeks of age, the earliest age at BMT in this study), could naturally explain the limited donor chimerism within memory subsets and, if they are less dynamic than displaceable memory populations, might also be able to explain host/donor differences in Ki67 expression.

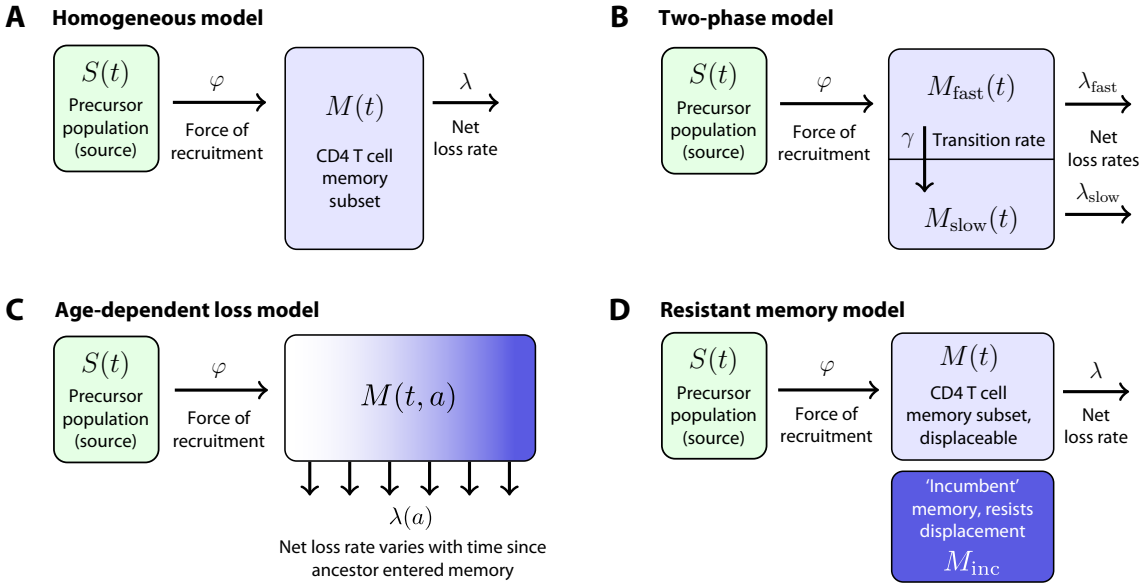

Figure 2: **Models of the generation and maintenance of memory CD4 T cell subsets in adult mice.** (**A**) New cells from a precursor (source) population of size $S(t)$ flow in to a homogeneous memory subset $M(t)$ at total rate $\varphi S(t)$. The force of recruitment φ is approximately the daily probability that any given cell from the source will be recruited into memory, multiplied by an expansion factor. This memory population may self-renew through division and be lost through death or differentiation, and is continually supplemented by cells from the source. We assume that the net loss rate (loss minus division) is a constant, λ, such that $1/\lambda$ is the mean lifetime of a memory clone. (**B**) In a two phase model of memory, new cells are recruited at rate $\varphi S(t)$ into a population $M_{\text{fast}}(t)$ that has a high net loss rate λ_{fast} and so is replaced by donor cells relatively quickly. These cells transition into a slower subset $M_{\text{slow}}(t)$ at constant rate γ and are then lost at net rate $\lambda_{\text{slow}} < \lambda_{\text{fast}}$. (**C**) The age-dependent loss model; here, the net loss rate of memory is a continuous function of cell 'age' a, defined as the time since a cell or its ancestor entered the memory pool. The model tracks the evolution of the population density of memory T cells of age a at host age t, $M(t,a)$. (**D**) In the resistant memory model, a subpopulation of 'incumbent' memory cells established early in life is stable in numbers.

The kinetics of accumulation of CD4$^+$ MP cells are consistent with a naive $\rightarrow$ T_{CM} $\rightarrow$ T_{EM} pathway, and both memory subsets are heterogeneous in their turnover

We compared the ability of the four mechanisms to describe the replacement kinetics of memory subsets in the dirty and clean environments. The kinetic of donor chimerism in CD4 T_{EM} clearly lagged that of CD4 T_{CM} (Fig. 1D), ruling out T_{EM} as a direct predictor of T_{CM} accumulation. We therefore considered only naive CD4 T cells as the source for T_{CM}, but considered both naive and T_{CM} cells as potential sources of T_{EM}.

For each environment (clean/dirty) and each subset (T_{EM}/T_{CM}), we then fitted each combination of source and model simultaneously to the timecourses of the total cell numbers and the proportion of donor cells within the subset. Full details of the models and fitting procedures are given in Methods and Materials.

We then calculated a measure of the combined probability (joint likelihood) that the replacement kinetics in both clean and dirty environments derive from that combination of source and model. We then used these joint likelihoods to assess our relative confidence in each combination of source and model, using the Akaike Information Criterion (see Methods). We found almost no support for the homogeneous or resistant memory models and clearly stronger support for T_{CM} cells rather than naive T cells as a predictor of T_{EM} production (Table 1). For T_{CM} the age-dependent loss was strongly favoured statistically, while for T_{EM} the two-phase model had the strongest support (fits shown in Fig. 3). However the two models gave visually very similar descriptions of each dataset (not shown). This similarity is perhaps unsurprising, as both describe a progressive increase in clonal persistence the longer cells or their progeny reside within the memory compartment.

		CD4 central memory	**CD4 effector memory**	
		Source population	Source population	
Model	Parameters	CD4 naive	CD4 naive	CD4 central memory
Homogeneous	3	**128** (10)	**89** (75)	**160** (39)
Two-phase	5	**9** (74)	**29** (109)	**0** (124)
Age-dependent loss	4	**0** (76)	**29** (107)	**10** (117)
Resistant memory	4	**26** (63)	**45** (99)	**49** (97)

Table 1: Measures of support (using differences in the Akaike information criterion, AIC - AIC_{min}; see Methods) for models in which CD4 T_{CM} derive directly from naive CD4 T cells, and T_{EM} derive either from naive T cells or T_{CM}. AIC differences are shown in bold, with zero indicating the model with strongest support and large AIC differences representing reduced support, with differences of 10 or more generally considered highly significant. Figures in parentheses are the log likelihoods, reflecting the quality of fit of each model. Indicated are the number of parameters estimated for each model in each environment.

Predicting the ontogeny of CD4$^+$ MP T cell subsets in clean mice

To challenge these models further, we used them to predict the kinetics with which memory CD4 T cell subsets develop early in life. We drew on measurements of naive and memory CD4 T cell numbers recovered from the spleen and lymph nodes of WT mice aged between 5 days and 15 weeks, kept in the clean facility (Fig. 4A). We assumed that the forces of recruitment into CD4 T_{CM} and T_{EM}, and the loss rate parameters for each subset, were the same as those estimated using data from clean adult mice. We solved each model using its fitted parameters and an empirical function $S(t)$ fitted to the timecourse of its appropriate source population (naive CD4 T cell numbers for T_{CM}, and T_{CM} numbers for T_{EM}; Fig. 4A). Starting from the mean numbers of CD4 T_{CM} and T_{EM} observed at age 5d, the trajectories predicted by the two-phase and age-dependent loss models tracked the observed growth in numbers of CD4 T_{CM} between 5d-15wk, which spanned two orders of magnitude, reasonably well (Fig. 4B, left panel). For CD4 T_{EM} the favoured two-phase model predicted their accumulation remarkably

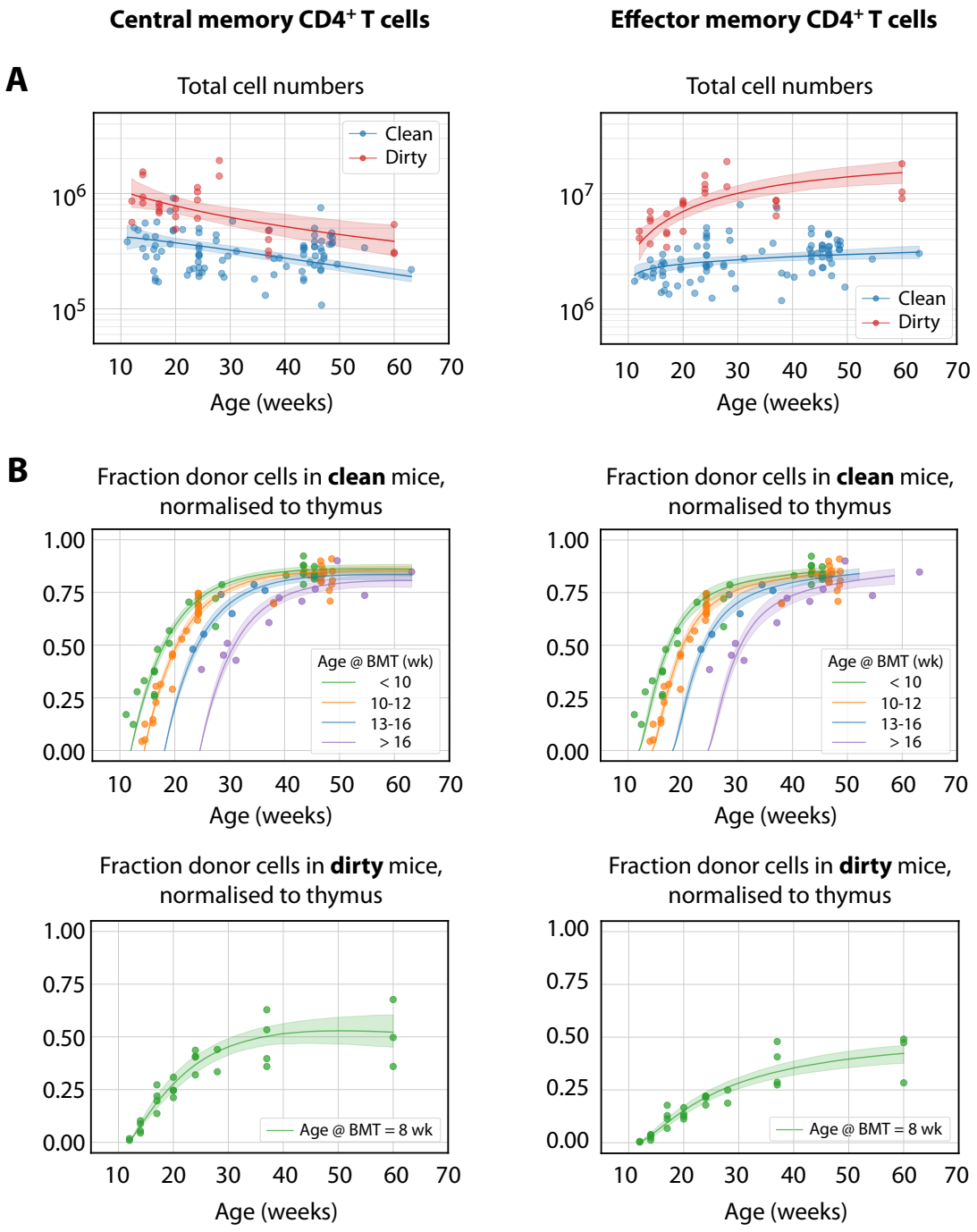

Figure 3: **The best-fitting models of memory dynamics.** The age-dependent loss model was the best description of T_{CM} dynamics, and the two-phase model best described T_{EM}. **(A)** Total (donor+host) numbers of memory T cells and **(B)** chimerism, from 4 weeks post bone marrow transplant (BMT). To visualise the fits, clean facility mice were grouped into small ranges of age at BMT, and the four curves show the model predictions for the median age within each group. All trajectories are described with the same parameters, differing only in the kinetics of the source population, which changes with mouse age. The lower panels show the fitted trajectories of CD4 T_{CM} and T_{EM} chimerism in mice in the dirty environment, all of which underwent BMT at a similar age.

accurately, while the age-dependent loss model performed relatively poorly (Fig. 4B, right panel). Despite the differences in statistical support for the two models in the two memory subsets, we remain somewhat equivocal regarding the true nature of heterogeneity in each, and present results below for both models. A robust conclusion, however, is that we find a progressive lengthening of clonal lifetimes in both memory subsets and environments, with newly recruited memory being lost on timescales of days to weeks, and more established memory persisting for several months (Fig. 5).

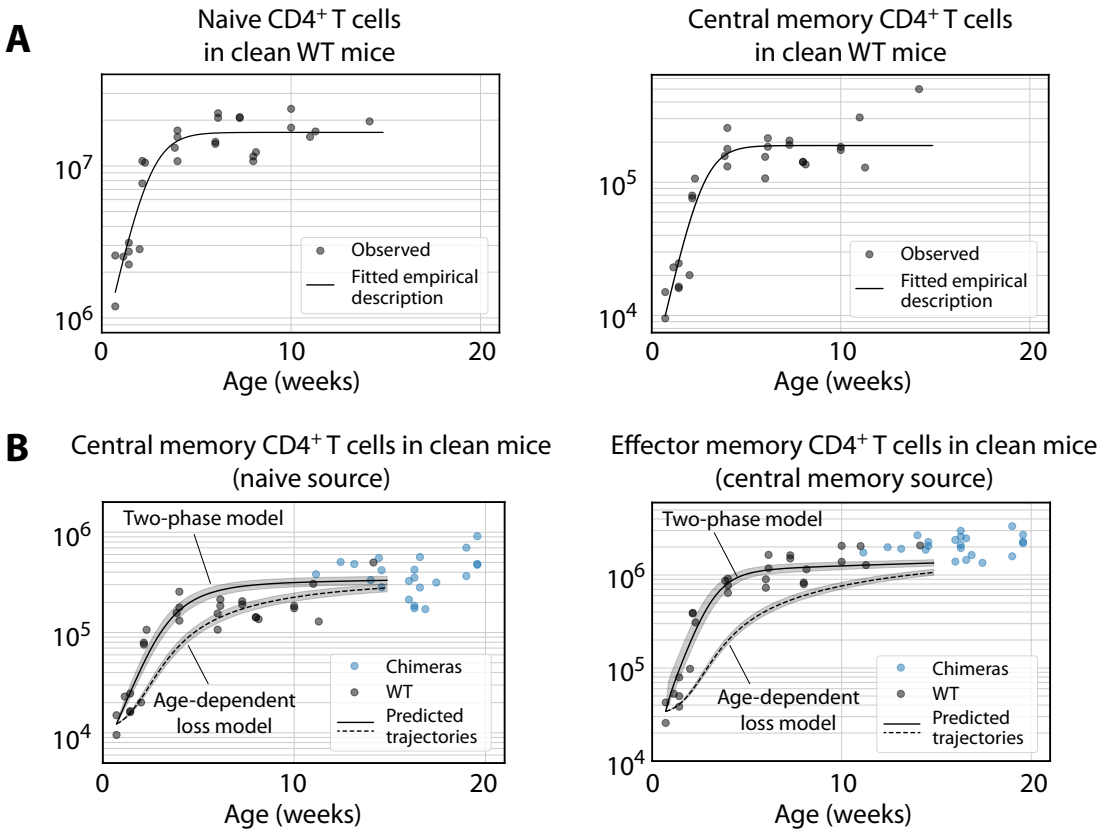

Figure 4: **Predicting the kinetics of development of memory CD4+ T cell compartments in clean mice.** **(A)** The timecourses of numbers of $CD4^+$ naive T cells and T_{CM} recovered from the spleen and lymph nodes of wild-type (WT) mice housed in the clean facility at UCL, aged 5 days to 15 weeks. We fitted the descriptor function $S(t) = S_{\max}/(1 + e^{-rt}(S_{\max} - S_{\min})/S_{\min})$ to both, using least squares and log-transformed observations, to model them as the sources of T_{CM} and T_{EM} subsets early in life. **(B)** Predicting the development of memory cell numbers in clean mice with the two-phase model (solid line) and age-dependent loss model (dashed line), using each model's estimated force of recruitment into memory, φ, and the loss rate parameters estimated in adults. Shaded regions indicate the spread of predictions over the 95% confidence intervals of the parameters. The black points (not used for fitting) are the numbers of CD4 T_{CM} and T_{EM} recovered from the spleen and lymph nodes of WT control mice in the same facility. Blue points denote cell numbers recovered from the busulfan chimeras, which were used to estimate the parameters for each model.

Constitutive generation of circulating CD4 T_{EM} and T_{CM} cells in adult mice occurs at constant rates, irrespective of environment

The kinetics of accumulation of donor-derived memory cells were visually indistinguishable in the two environments from age 10 weeks onwards (Fig. 1C), suggesting similar net rates of recruitment and loss. Consistent with this observation, we found no significant differences between clean and dirty mice in the forces of recruitment

(φ) into circulating CD4 T cell memory subsets between the ages of 11-64 weeks, in either model, and no substantial differences in their rates of loss (Fig. 5 and Table 2). Therefore, we infer that antigenic stimuli common to both environments drive the continuous generation of new effector and central memory CD4 T cells in adult mice, at total rates that are proportional to the sizes of their precursor populations.

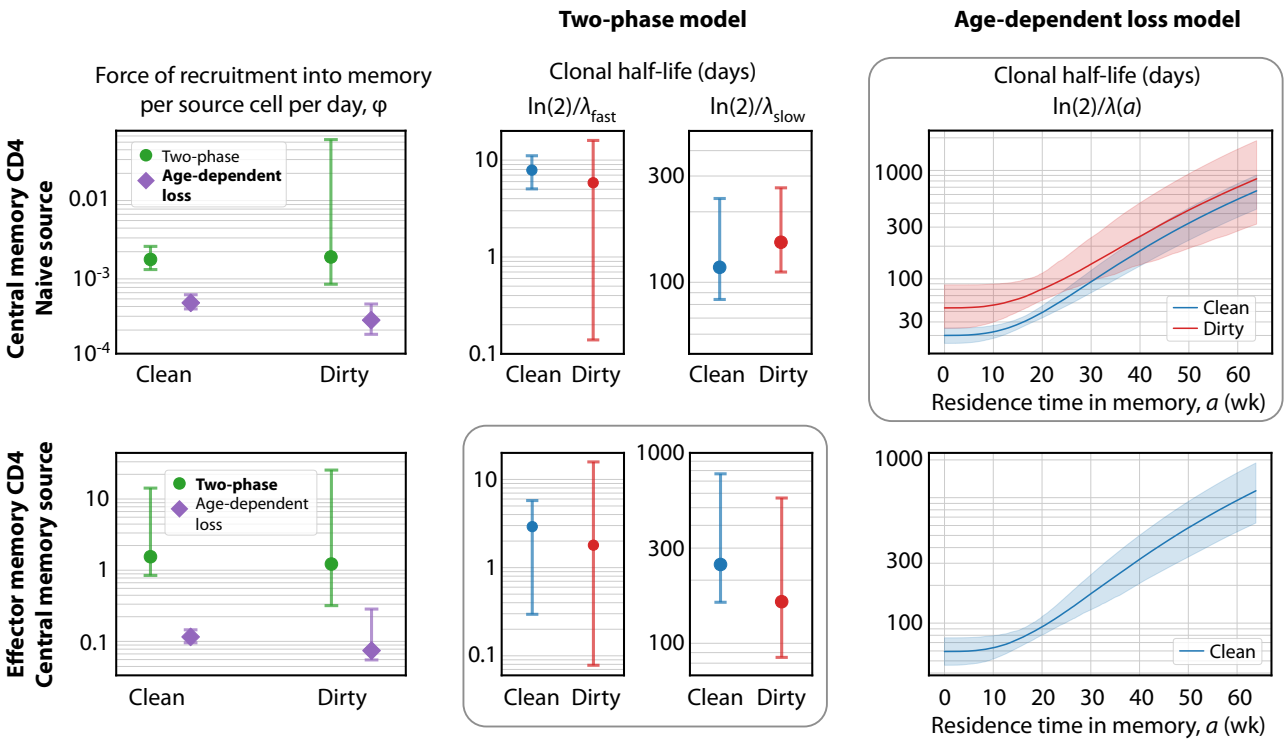

Figure 5: **Key parameters describing the constitutive production of central and effector memory CD4 T cells in adult mice**. **Left panels:** Estimates of the *per capita* rate of recruitment from the source (φ) for each model and each population. Vertical bars represent bootstrapped 95% confidence intervals. The favoured model for each population is indicated in bold in the legend. **Middle panels:** The estimated clonal half-lives of fast and slow memory in the two-phase model. The enclosing box indicates that this model was favoured for T_{EM}. **Right panels:** The estimates of clonal half-life derived from the age-dependent loss model, favoured for T_{CM}. For T_{EM} in dirty mice, the estimated $\lambda(a)$ was close to zero. All parameter estimates are given in Table 2.

Quantifying the long-term dynamics of CD4$^+$ MP subsets

Our analyses give a quantitative picture of recruitment into memory and the cells' subsequent life-histories, and allow us to identify features of their population dynamics that are common to both environments and model-independent. First, the donor chimerism in T_{CM} reached substantially lower levels than the naive CD4 T cell precursors (Fig. 1D), suggesting that the rate of generation of new memory in both environments wanes with age, and/or that more established memory resists displacement. We find evidence for both processes here. We show in Methods and Materials that if influx declines faster than the average rate of turnover, a population will be unable to reach the same level of chimerism as its precursor – in effect, the flow from the source 'dries up' more quickly than the memory pool is renewed by immigrants. We see signs of this effect; due to thymic involution, naive CD4 T cell numbers decay exponentially in both clean and dirty adult mice (Fig. 1B) with population half lives of 228 days (95% CI 227-231 days) and 143 (142-144) days respectively. These timescales are comparable to or shorter than the estimated half lives of established T_{CM} memory clones ($\ln(2)/\lambda_{slow}$ in the two-phase model; and $\ln(2)/\lambda(a)$ for $a > 30$ weeks in the age-dependent loss model; Fig. 5 and Table 2). In addition, both the

two-phase and age-dependent models indicate that older memory clones have a fitness advantage over newer ones. Therefore, the limited chimerism in CD4 T_{CM} derives from the decline in naive T cell numbers with age, slow average rates of turnover, and the increased persistence of established memory cells. This slow rate of accumulation of new T_{CM} in turn acts to limit the chimerism observed in T_{EM}, which are also lost slowly.

			CD4 T_{CM}		**CD4 T_{EM}**	
Model	Parameter	Quantity	Clean	Dirty	Clean	Dirty
Two-phase	Force of recruitment (d^{-1})	φ	1.4 (1.2, 2.3) $\times 10^{-3}$	1.5 (0.77, 54) $\times 10^{-3}$	1.2 (0.76, 12)	1.1 (0.29, 23)
	Daily cell influx at age $t^* = 20$ wk	$\varphi S(t^*)$	2.3 (2.0, 3.9) $\times 10^4$	3.2 (1.7, 120) $\times 10^4$	36 (22, 370) $\times 10^4$	84 (21, 1700) $\times 10^4$
	Net loss rate of fast subset (d^{-1})	λ_{fast}	0.082 (0.063, 0.14)	0.103 (0.043, 5.2)	0.23 (0.12, 2.4)	0.39 (0.045, 9.0)
	Net loss rate of slow subset (d^{-1})	λ_{slow}	5.9 (3.01, 9.4) $\times 10^{-3}$	4.8 (2.7, 6.9) $\times 10^{-3}$	2.5 (0.81, 4.6) $\times 10^{-3}$	4.8 (1.01, 8.8) $\times 10^{-3}$
	Half-life of fast subset (d)	$\ln(2)/\lambda_{fast}$	8.4 (5.04, 11)	6.7 (0.14, 16)	3.02 (0.30, 5.8)	1.8 (0.078, 16)
	Half-life of slow subset (d)	$\ln(2)/\lambda_{slow}$	120 (75, 230)	140 (101, 260)	270 (150, 770)	140 (75, 570)
	% of memory transitioning to slow	$100\gamma/(\lambda_{fast} + \gamma)$	3.4 (0.46, 4.1)	5.0 (0.18, 10)	1.8 (0.21, 2.4)	9.1 (0.36, 38)
	Proportion slow at t^* =20 wk	$M_{slow}(t^*)/M(t^*)$	0.25 (0.12, 0.30)	0.61 (0.45, 0.75)	0.36 (0.25, 0.41)	0.72 (0.41, 0.87)
Age-dependent	Force of recruitment (d^{-1})	φ	0.43 (0.38, 0.57) $\times 10^{-3}$	0.26 (0.18, 0.43) $\times 10^{-3}$	0.10 (0.086, 0.13)	0.062 (0.049, 0.26)
loss	Daily cell influx at age $t^* = 20$ wk	$\varphi S(t^*)$	0.70 (0.62, 0.93) $\times 10^4$	0.57 (0.39, 0.96) $\times 10^4$	3.04 (2.5, 3.8) $\times 10^4$	4.6 (3.7, 19) $\times 10^4$
	Net loss rate of new memory (d^{-1})	λ_0	2.2 (2.0, 2.7) $\times 10^{-2}$	1.2 (0.79, 2.0) $\times 10^{-2}$	1.2 (0.91, 1.5) $\times 10^{-2}$	1.1 (-44, 26) $\times 10^{-5}$
	Memory age threshold† (d)	A	150 (140, 200)	190 (130, 310)	150 (130, 230)	NA

Table 2: **Estimates of parameters governing CD4 T_{CM} and T_{EM} homeostasis in adult mice**. †In the age-dependent loss model, the threshold cell age A defines the beginning of the more persistent phase of memory maintenance ($\lambda(a) = \lambda_0/(1 + (a/A)^3)$); estimates of λ_0 for T_{EM} in dirty mice were close to zero, and A was poorly constrained.

One can also quantify the fates of populations after entering memory, although here our insights are more model-dependent. The two-phase model predicts that the process of establishment of memory is relatively inefficient, with 'fast' memory cells lost over timescales of days and only a small proportion of these surviving to become more persistent 'slow' memory (∼2-10% of T_{EM}, and ∼3-5% of T_{CM}; Table 2). Despite this inefficiency, the substantial constitutive influxes maintain the fast and slow subpopulations at comparable sizes, consistent with our previous analysis of BrdU labelling of CD4 T_{CM} and T_{EM} in WT mice (Gossel *et al.*, 2017). In contrast, the age-dependent loss model makes lower estimates of the force of recruitment into memory (Fig. 5, left panels) but predicts a more efficient transition, with newly generated memory having clonal half-lives of 20-40 days and a much greater proportion of memory persisting longer-term (Fig. S3).

Larger memory populations in dirty mice derive from early antigen exposure

Given the similarity of the rates of generation of memory in clean and dirty adult mice, and of their rates of turnover, we infer that the larger, stable memory populations in dirty mice (Fig. 3A) must derive from the early establishment of greater numbers of both T_{CM} and T_{EM}. This difference is then sustained well into adulthood by the very slow loss of these early memory populations.

To explore this hypothesis, we used the best fitting model of T_{CM} dynamics in adult mice in the dirty facility, the age-dependent loss model, with the timecourse of naive CD4 T cells early in life (Fig. 4A) to predict their kinetics of accumulation of T_{CM}. The trajectory underestimated their numbers in adults by a factor of approximately 4 (Fig. 6). which in turn made an even more substantial underestimate of the accumulation of T_{EM} (not shown). This prediction was insensitive to the presumed numbers of T_{CM} at age 5d, because they are rapidly outnumbered by the influx of new memory cells from the exponentially expanding naive CD4 T cell pool. We conclude that an additional force early in life, presumably deriving from increased exposure to environmental antigens, is required to account for the increased memory T cell numbers in adulthood in the dirtier facility.

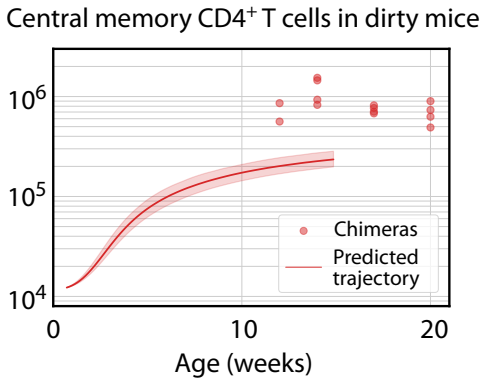

Figure 6: **Predicting the establishment of the CD4 T_{CM} in dirty mice**. The age-dependent loss model of memory CD4 T cell homeostasis in adult mice in dirty facilities underestimates the rate of accumulation of T_{CM} early in life.

Analysis of germ free mice confirms roles for both autoreactive and commensal stimuli in the establishment of memory compartments

We found that the rate of constitutive recruitment into memory in adult mice was insensitive to variations in environmental commensals, and that these antigens must exert their biggest influence on the establishment of MP cells in neonates and young mice. However, earlier studies reported that numbers of memory cells in the spleens of SPF and germ-free (GF) mice are similar and argue that self-recognition is therefore the sole driver of MP cell generation in early life (Kawabe *et al.*, 2017). To reconcile these apparent differences, and dissect the contributions of self and foreign antigens to the establishment of MP T cells in young mice, we compared the size and behaviour of memory CD4 T cell subsets in C57Bl6/J and/or C57Bl6/SJL mice housed in a wider range of environments. In addition to the clean (UCL) and dirty (NIMR) mice analysed above, we enumerated cells from GF and SPF mice obtained from the Kennedy Institute (KI) in Oxford. Consistent with these earlier studies, substantial numbers of both T_{CM} and T_{EM} MP cells were recovered from GF mice aged between 40-200d, confirming that the generation of MP cells does not depend exclusively on commensal-derived foreign antigens (Fig. 7A). However, the memory CD4 T cell compartments of GF mice, enumerated from spleen and lymph nodes combined, were significantly smaller than in the SPF mice in all facilities. Clean mice from KI and UCL had similar-sized memory compartments, and in turn both were substantially smaller than those in mice from the dirty facility (NIMR) (Fig. 7A). Indeed the dirty mice played host to around five times the number of MP cells found in GF mice, indicating that antigens from commensal organisms are a substantial driver of MP cell expansion.

We also analysed the proliferative activity of MP cells in mice from the different environments, by measuring the expression of Ki67. Division of MP cells is dependent on TCR (Seddon *et al.*, 2003) and CD28 costimulation signaling (Kawabe *et al.*, 2017). A substantial fraction of MP cells in GF mice expressed Ki67 (Fig. 7B), indicating cell cycle activity within the previous 3-4 days (Gossel *et al.*, 2017). This proportion was broadly similar to that in mice from both clean and dirty environments, indicating that the level of proliferation of CD4 MP T cells in adult mice was relatively insensitive to environmentally-derived stimuli.

Quantifying the forces exerted by commensals on memory generation early in life

Finally, we compared the rates of memory generation in young mice in the different environments. We began with the favoured age-dependent loss model of T_{CM} dynamics. Using the parameters from clean adult mice

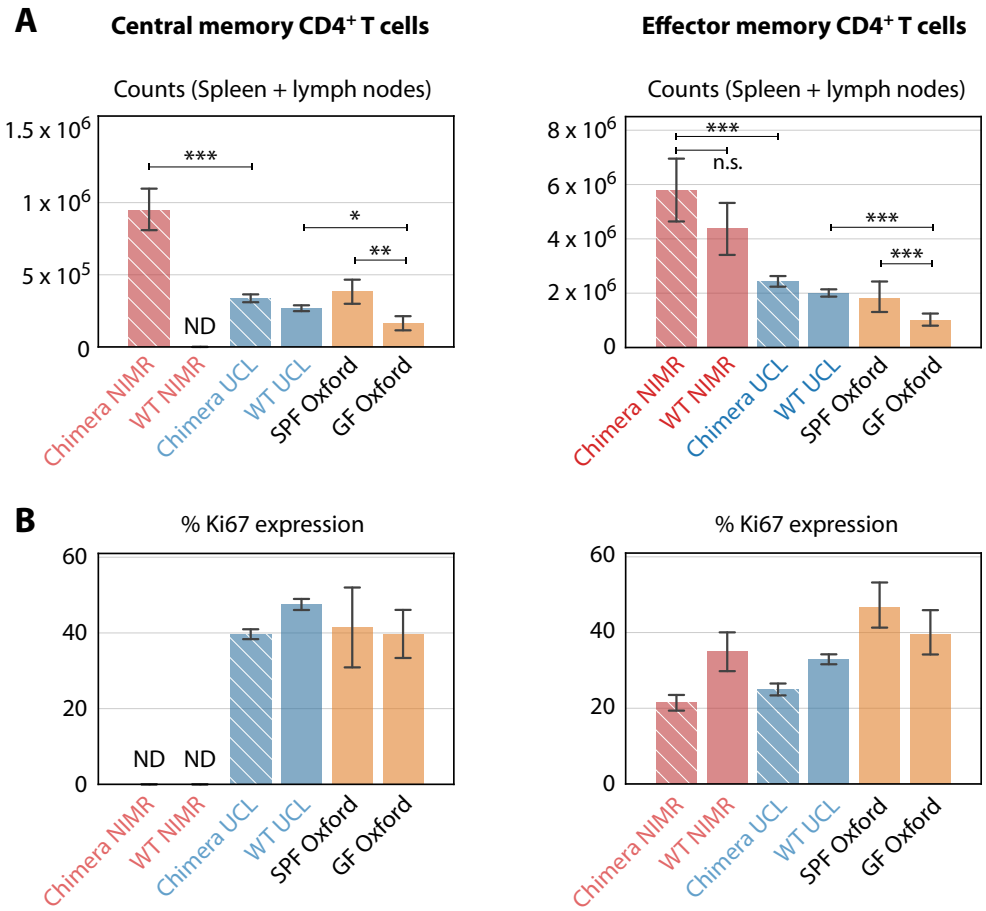

Figure 7: **Comparing numbers (A) and proliferative activity (B) of CD4 T_{CM} and T_{EM} in adult mice in different SPF and GF facilities.** Cross-hatched bars denote busulfan chimeras, solid bars WT mice. NIMR (red bars) and UCL (blue bars) are the 'dirty' and 'clean' facilities used for the bulk of the analysis presented here. 'ND' denotes data not available. * $p < 0.05$, ** $p < 0.01$, *** $p < 0.001$, using the Mann-Whitney test. Group sizes: Panels A; (28, 0, 78, 102, 4, 14) and (46, 11, 78, 91, 4, 14). Panels B; (0, 0, 74, 140, 4, 14) and (18, 4, 74, 140, 4, 14).

(which were similar to those estimated for dirty mice, and for which no estimates were available for GF mice), and the empirical description of naive CD4 T cell numbers in clean WT mice (Fig. 4A), we then estimated the fold changes in the force of recruitment φ needed during the first 11 weeks of life needed to seed CD4 T_{CM} at the average numbers observed the mice aged between 11 and 28 weeks. Memory cell numbers were relatively stable in all facilities during this period (Fig. 8, left panel). GF mice needed approximately 0.4 times the force of recruitment in clean adult mice, younger clean mice needed a force approximately 1.1 times greater than in adults, and dirty mice required a force 2.7 times greater. As before, uncertainty in memory cell numbers at age 5d had very little effect on the predicted levels of memory attained at week 11, or on these estimated correction factors.

We then used these environment-specific, corrected trajectories of T_{CM} development to predict the accumulation of T_{EM} by age 11 weeks, using the favoured two-phase model. Remarkably, after accounting for the different T_{CM} population sizes, the force of recruitment from T_{CM} to T_{EM} estimated in clean adult mice was also sufficient to account for T_{EM} numbers in all three environments (Fig. 8, right panel).

In summary, this analysis showed that approximately 2- to 3-fold increases or decreases in the force of recruitment into CD4 T_{CM} observed in clean adult (UCL) mice were sufficient to explain their numbers in dirty mice from NIMR or GF mice. However the subsequent rate of development of T_{EM} from T_{CM} appeared to be independent of both mouse age and environment, and differences in the numbers of T_{EM} could be explained simply by the differences in the size of the T_{CM} precursor population. These results suggest that the rate of generation of CD4 T_{CM} from naive T cells in young mice reflects both self antigens and the level of exposure to environmental antigens, but that differentiation from T_{CM} to T_{EM} appears to be largely insensitive to these forces.

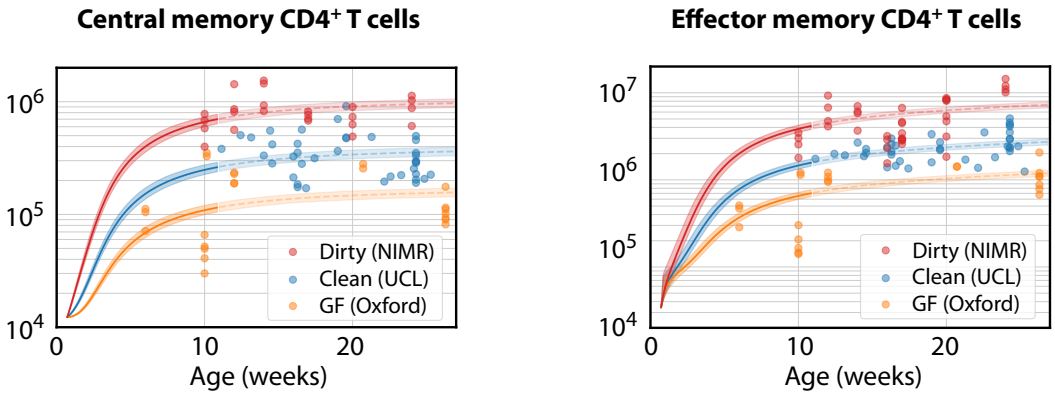

Figure 8: **Modelling the ontogeny of CD4 memory T cell subsets at different facilities**. As in Fig. 4B, we took the parameters estimated for clean (UCL) adult mice and used them together with naive CD4 T cell numbers to predict the kinetic of accumulation of CD4 T_{CM} from age 5d onwards (blue curve). Using these parameters, we estimated a correction to the force of recruitment φ early in life needed to generate the observed memory cell numbers in all three environments (left panel). To do this we fitted the trajectories, with the correction factor as the single unknown, to available data from these facilities from mice up to 28 weeks of age. Then we used those these corrected CD4 T_{CM} trajectories to predict the numbers of CD4 T_{EM} in adult mice in each environment Dashed lines show the projection as far as 27 weeks.

Discussion

In this study, we compared mice housed in facilities with distinct antigenic burdens to investigate the nature and timing of the forces that establish and maintain MP CD4 T cell compartments. We examined (i) tonic recruitment into the T_{CM} and T_{EM} pools in adults, (ii) the kinetic substructure and maintenance of these compartments throughout life, and (iii) the generation/establishment of the compartment early in life. Our analyses indicate that self recognition contributes to all these processes, but that the contribution of reactivity to commensals is largely restricted to the neonatal period.

Our analysis of GF mice, which lack exposure to commensal organisms, confirmed earlier work showing that generation of MP cells in adults is not driven exclusively by foreign commensals (Kawabe *et al.*, 2017) and suggesting that self-recognition is instead the key driver. While GF mice lack exposure to live organisms, they are not entirely free of environmental antigens and it is possible that proteins in bedding material and diet could represent foreign antigenic stimuli. However, the argument for self-recognition is made through the correlation of the degree of MP cell conversion and steady state proliferation with affinity for self-MHC, as indicated by CD5 expression. We also found that memory CD4 T cell division, as reported by Ki67, was substantial and largely independent of the level of commensals. We could not determine the extents to which Ki67 expression derived from the homeostatic proliferation of existing cells or the influx of newly generated MP cells. However, the common levels of Ki67 across environments, together with our findings from the adult clean and dirty chimeric mice that the rates of memory generation and net loss were insensitive to environment, support our conclusion that self-recognition is the major driver of both recruitment and proliferative renewal in adult memory compartments.

Commensals did, however, have a substantial impact upon the sizes of the memory compartments generated early in life. CD4 T_{CM} and T_{EM} numbers in mice raised in dirty environments were 3-5 times greater than those in either GF or cleaner IVC or SPF facilities, and these differences could be explained by differences in the forces of recruitment of CD4 T_{CM} during ontogeny. The estimated 7-fold difference in this force between GF and dirty mice prompts the simple interpretation that self-recognition only accounts for $\sim$14% of the memory compartment in dirty mice.

We ascribe differences in memory compartment sizes to different commensal burdens, but it is possible that their smaller sizes in GF mice also derive from their smaller lymph nodes (LN). Bacterial stimulation of DCs is required for their migration into LN and these DCs are required for normal LN development (Moussion and Girard, 2011, Wendland *et al.*, 2011, Zhang *et al.*, 2016). Therefore, it is not straightforward to separate the indirect influence of commensals on lymphoid development from any direct influences upon memory generation. It is also possible that some of the additional force of recruitment in neonates derives not from commensals but from lymphopenia, which can drive naive T cells to acquire a memory phenotype (Min *et al.*, 2003). However, this process was demonstrated by transferring naive cells from adults into very young mice, so it is possible that such naive cells do not represent the activity of neonatal naive T cells, which are almost exclusively RTE.

We observed that environment not only impacted memory but also naive T cells. Their numbers naturally decline with age, but this decline was almost twice as fast in dirty mice than in genetically identical mice housed in cleaner facilities (Fig. S2; numbers halve every 228 days (95% CI 227-231) in clean mice, and 143d (142-144) in dirty mice). This difference likely derives from more rapid reduction in thymic output with age in the dirty environment, and not differences in lifespans of naive CD4 T cells in the two environments, because we see similar rates of decline in the numbers of single positive SP thymocytes at the latest stage of thymic development (halving every every 282d (281-308) in clean mice, 151d (150-159) in dirty mice; data not shown). Therefore, it appears that another consequence of life in a more antigenically diverse environment is more rapid involution of the thymus. It is possible that this effect derives from the stress or inflammation associated with an increased commensal burden, or is a consequence of expanded memory populations; but whatever the mechanism, our

data clearly indicate that environmental factors can impact the maintenance of naive T cells.

Our models do not incorporate any homeostatic regulation in the sense of feedback control of division or loss through quorum sensing. Since memory cell numbers only vary by a factor of 2-3 between clean and dirty mice these mice, we did not expect to detect any strong variation in net loss rate with pool size with these data, and indeed our estimates of loss rates were similar in the two environments. While we cannot rule it out at higher cell densities, there is arguably little evidence for homeostatic regulation of memory in SPF mice. We observed a range of relatively stable memory compartment sizes in the different containment facilities; memory pools do not 'fill up' with large clones in very young mice, which might occur if rates of division or loss were very sensitive to total pool size; and memory compartments appear to be expandable following multiple infections in older animals (Vezys *et al.*, 2009).

Our modelling approach yielded robust conclusions regarding the nature and magnitudes of the forces generating CD4 T_{CM} and T_{EM}, and the existence of heterogeneity within each subset, consistent with previous reports by ourselves and others of subpopulations of CD4 MP cells with distinct rates of division and turnover (Gossel *et al.*, 2017, Younes *et al.*, 2011). However, these models are abstractions and resolving the details of kinetic substructure in lymphocyte populations is challenging (Ganusov *et al.*, 2010). For CD4 T_{CM} in adult mice we found evidence for slow and continuous changes in their net loss rates as cells age, and additional support for such a process comes from the slow rate at which Ki67 levels in donor and host memory cells converge in adult busulfan chimeras. In contrast, the data for T_{EM} in adult mice, and the predictions of the growth in both subsets in younger mice, more strongly supported a discrete two-phase model with a relatively rapid transition from fast to slow memory at a rate that appears constitutive and insensitive to environment. Characterising the homeostatic dynamics of CD4 T cell memory and how they change with age requires further study.

Methods and Materials

Generating busulfan chimeric mice

Mice were treated with optimised low doses of busulfan to deplete HSC but leave peripheral T cell subsets intact. HSC were reconstituted with congenically-labelled, T-cell depleted bone marrow to generate stable chimeras (Fig. 1A). Details of the protocols are given in (Hogan *et al.*, 2017b) and (Hogan *et al.*, 2017a).

Mice

Busulfan chimeric mice and wildtype control mice were housed in conventional animal facilities, either at the National Institute for Medical Research, London, UK (NIMR); or at the UCL Royal Free Campus, London, UK (UCL). At NIMR, mice were housed in open cages and drank tap water. At UCL, mice were housed in individually ventilated cages and drank irradiated water. Germ Free and SPF mice were housed at the Oxford Centre for Microbiome Studies, Oxford, UK.

Flow cytometry

Single cell suspensions were prepared from the thymus, spleen and lymph nodes of busulfan chimeric mice, wildtype control mice, or germ free mice. Cells were stained with the following monoclonal antibodies and cell dyes: CD45.1 FITC, CD45.2 FITC, CD45.2 AlexaFluor700, TCR-β APC, CD4 PerCP-eFluor710, CD44 APC-eFluor780, CD25 PE, CD25 eFluor450, CD25 PE-Cy7, CD62L eFluor450, NK1.1 PE-Cy7 (all eBioscience),

CD45.1 BV650, CD45.2 PE-Dazzle, TCR-β PerCP-Cy5.5 CD4 BV711, CD44 BV785, CD25 BV650 (all Biolegend), CD62L BUV737 (BD Biosciences), LIVE/DEAD nearIR and LIVE/DEAD blue viability dyes. For Ki67 staining, cells were fixed using the eBioscience Foxp3/ Transcription Factor Staining Buffer Set and stained with either anti-mouse Ki67 FITC or PE (both eBioscience). Cells were acquired on a BD LSR-II or a BD LSR-Fortessa flow cytometer and analysed with Flowjo software (Treestar). Conventional CD4 cells were identified as live TCR-β+ CD4+ CD25- NK1.1-, and then CD44 and CD62L were used to identify EM (CD44+CD62L-) and CM (CD44+CD62L+) subsets.

Modelling the fluxes between naive, central memory and effector memory CD4 subsets

The homogeneous model

Our simplest description of the kinetics of the generation and renewal of CD4 T_{CM} and T_{EM} is illustrated in Fig. 2A and was formulated as follows. We assume that cells flow into a memory subset of total size $M(t)$ from a precursor population $S(t)$ at total rate $\varphi S(t)$, where t is the age of the animal. The rate constant φ is the 'force of recruitment', a compound parameter which is the product of the *per capita* rate of recruitment of cells from the source population per day multiplied by number representing any net expansion that occurs during recruitment. Memory is also lost at net *per capita* rate λ. This rate is the balance of loss through death and/or differentiation, and any compensatory cell production through division, and represents the rate of decline of (at least partly) self-renewing populations, rather than the loss rate of individual cells. We place no constraints on these rates, and so λ may be positive or negative.

$$\frac{dM(t)}{dt} = \varphi S(t) - \lambda M(t). \tag{1}$$

We assume host and donor cells each obey the same kinetics, so that

$$\frac{dM_{\text{host}}(t)}{dt} = \varphi S_{\text{host}}(t) - \lambda M_{\text{host}}(t) \tag{2}$$

$$\frac{dM_{\text{donor}}(t)}{dt} = \varphi S_{\text{donor}}(t) - \lambda M_{\text{donor}}(t), \tag{3}$$

where the total population size $M(t) = M_{\text{donor}}(t) + M_{\text{host}}(t)$. Our strategy for parameter estimation was to fit this model simultaneously to the timecourses of total numbers of memory cells $M(t)$, and the donor chimerism within memory, $\chi_{\text{M}}(t)$, which is the fraction of cells in memory that are donor-derived. For reasons described below, we normalise this fraction to the proportion of early double-positive (DP1) thymocytes that are donor-derived, which is measured in the same mouse and denoted χ_{DP1};

$$\chi_{\text{DP1}} = \frac{\text{DP1}_{\text{donor}}}{\text{DP1}_{\text{host+donor}}}, \quad \chi_M(t) = \frac{M_{\text{donor}}(t)}{M(t)}, \quad \chi_{\text{M, norm}}(t) = \frac{\chi_M(t)}{\chi_{\text{DP1}}}. \tag{4}$$

Eqns. 2 and 3 then give

$$\frac{d}{dt}\chi_{\text{M, norm}}(t) = \frac{d}{dt}\left(\frac{M_{\text{donor}}(t)}{\chi_{\text{DP1}}(t)M(t)}\right) = \frac{1}{\chi_{\text{DP1}}(t)}\frac{d}{dt}\left(\frac{M_{\text{donor}}(t)}{M(t)}\right) - \frac{d\chi_{\text{DP1}}/dt}{\chi_{\text{DP1}}(t)^2}\left(\frac{M_{\text{donor}}(t)}{M(t)}\right). \tag{5}$$

If observations are made sufficiently long after BMT (more than approximately 4 weeks), chimerism among DP thymocytes can be assumed to have stabilised (Hogan *et al.*, 2015a) and so we can neglect the term in $d\chi_{\text{DP1}}/dt$.

Then

$$\begin{aligned}
\frac{d}{dt}\chi_{\text{M, norm}}(t) &= \frac{1}{\chi_{\text{DP1}}M(t)}\left(\varphi S_{\text{donor}}(t) - \lambda M_{\text{donor}}(t) - \frac{M_{\text{donor}}(t)}{M(t)}\frac{dM(t)}{dt}\right) \\
&= \frac{1}{\chi_{\text{DP1}}M(t)}\left(\varphi S_{\text{donor}}(t) - \lambda M_{\text{donor}}(t) - \chi_M(t)\left(\varphi S(t) - \lambda M(t)\right)\right) \\
&= \frac{1}{\chi_{\text{DP1}}M(t)}\left(\varphi S_{\text{donor}}(t) - \chi_M(t)\varphi S(t)\right) \\
&= \frac{\varphi S(t)}{M(t)}\left(\chi_{\text{source, norm}}(t) - \chi_{\text{M, norm}}(t)\right), \qquad (6)
\end{aligned}$$

where we define

$$\chi_{\text{source, norm}}(t) = \frac{1}{\chi_{\text{DP1}}}\frac{S_{\text{donor}}(t)}{S(t)}. \qquad (7)$$

By normalising the chimerism of both the source and the memory populations to that in the thymus, we remove any variation in these quantities due to variation across individuals in the degree of chimerism achieved with busulfan treatment and BMT.

Fitting required initial conditions for the total numbers of memory cells and donor chimerism. We solved all of the models from host age t_0, which was chosen to be the time at which donor chimerism in memory for the mouse with the youngest age at BMT could be assumed to be zero and donor chimerism in DP1 had stabilised. This was host age 66d for the clean mice and 84 days for dirty mice (26d and 28d post-BMT respectively). Our results were insensitive to changes of a few days in these baseline ages. We also required functional forms for the kinetics of the source population $S(t)$ and $\chi_{\text{source, norm}}(t)$. When considering naive CD4 T cells as the source of both T_{CM} and T_{EM}, naive CD4 T cell numbers from age t_0 onwards in both facilities were well described with exponential decay, $S(t) = S(t_0)e^{-\nu t}$, though with different exponents (Fig. S2A). With this form we can solve eqn. 1 for $M(t)$ explicitly;

$$\begin{aligned}
M(t) &= M(t_0)e^{\lambda(t_0-t)} + \int_{s=t_0}^{t}\varphi S(s)e^{-\lambda(t-s)}ds \qquad (8) \\
&= M(t_0)e^{\lambda(t_0-t)} + \varphi S(t_0)e^{-\lambda t}\int_{s=t_0}^{t} e^{-(\nu-\lambda)s}ds \\
&= M(t_0)e^{\lambda(t_0-t)} + \frac{\varphi S(t_0)}{\lambda-\nu}(e^{-\nu t} - e^{\lambda(t_0-t)-\nu t_0}). \qquad (9)
\end{aligned}$$

Using this expression for $M(t)$ in eqn. (6), the kinetics of normalised chimerism in memory are

$$\begin{aligned}
\frac{d}{dt}\chi_{\text{M, norm}}(t) &= \frac{\varphi S(t_0)e^{-\nu t}}{M(t_0)e^{\lambda(t_0-t)} + \frac{\varphi S(t_0)}{\lambda-\nu}(e^{-\nu t} - e^{\lambda(t_0-t)-\nu t_0})} \times \left(\chi_{\text{source, norm}}(t) - \chi_{\text{M, norm}}(t)\right) \\
&= \frac{1}{e^{(\nu-\lambda)t}\left(\frac{e^{-(\nu-\lambda)t_0}}{\nu-\lambda} + \frac{M(t_0)e^{\lambda t_0}}{\varphi S(t_0)}\right) - \frac{1}{\nu-\lambda}} \times \left(\chi_{\text{source, norm}}(t) - \chi_{\text{M, norm}}(t)\right). \qquad (10)
\end{aligned}$$

The rate of increase in donor chimerism in memory then depends on the force of recruitment φ, the dynamics and chimerism of the source $S(t_0)e^{-\nu t}$ and $\chi_{\text{source, norm}}(t)$, the initial memory pool size $M(t_0)$, and the net loss rate λ. Note that eqn. (10) predicts that given sufficiently long, and if the rate of decline of naive T cells is slower than the rate of loss of memory ($\nu < \lambda$), the chimerism in memory will stabilise at the chimerism of naive CD4 T cells.

When considering T_{CM} as a source for T_{EM} we described $S(t)$ with either a sigmoid or exponential decay curve

(Fig. S2B). We described each source's chimerism with a generalised logistic function (Fig. S2C and D).

The homogeneous model is characterised by the three unknowns $M(t_0)$, λ and φ. To estimate them for a given subset, location and source population we solved eqns. 1 and 6 numerically and fitted them simultaneously to the timecourses of total numbers and normalised chimerism of the memory subset. The clean mice underwent BMT at a range of ages, which were accounted for individually in the fitting; model predictions for a mouse which underwent BMT at age t_B and was observed at age t were generated by running the model from host age $T = t_b+$ 26d (clean) or t_b+ 28d (dirty) to time t; with $M(T)$ calculated from $M(t_0)$ using eqn. 8, and the normalised chimerism at time T assumed to be zero. To estimate parameters we used the reduced likelihood approach described in Hogan *et al.* (2015b). Memory cell numbers were log-transformed and chimerism values were arcsine-square-root transformed to normalise the distributions of residuals. We estimated 95% confidence intervals on parameters by bootstrapping residuals 1000 times, and taking the 2.5% and 97.5% quantiles of the resulting sample of parameter estimates.

The two-phase model

The two-phase model (Fig. 2B) describes the kinetics of CD4 T_{CM} and T_{EM} assuming that both comprise two subpopulations with distinct rates of loss,

$$M(t) = M_{\text{fast}}(t) + M_{\text{slow}}(t), \tag{11}$$

where t is the mouse age. We assume that cells flow only into one subset from the precursor population $S(t)$ at total rate $\varphi S(t)$, and transition to the next compartment at rate γ;

$$\begin{aligned} \frac{dM_{\text{fast}}(t)}{dt} &= \varphi S(t) - \gamma M_{\text{fast}}(t) - \lambda_{\text{fast}} M_{\text{fast}}(t) \\ \frac{dM_{\text{slow}}(t)}{dt} &= \gamma M_{\text{fast}}(t) - \lambda_{\text{slow}} M_{\text{slow}}(t). \end{aligned} \tag{12}$$

Note that despite the nomenclature, when estimating the rates of loss of these subsets, we did not constrain them; rather, the model fits indicated that the upstream population has the greater net rate of loss.

Assuming that host and donor cells obey the same kinetics, so that eqns. 12 hold identically for both populations, then similar to the derivation of eqn. 6 we obtain the following equations for the dynamics of donor chimerism in the fast and slow subsets, each normalised to the chimerism of DP1 thymocytes;

$$\begin{aligned} \frac{d}{dt}\chi_{\text{fast, norm}}(t) &= \frac{\varphi S(t)}{M_{\text{fast}}(t)}(\chi_{\text{source, norm}}(t) - \chi_{\text{fast, norm}}(t)) \\ \frac{d}{dt}\chi_{\text{slow, norm}}(t) &= \frac{\gamma M_{\text{fast}}(t)}{M_{\text{slow}}(t)}(\chi_{\text{fast, norm}}(t) - \chi_{\text{slow, norm}}(t)), \end{aligned} \tag{13}$$

where

$$\chi_{\text{fast, norm}}(t) = \frac{1}{\chi_{\text{DP1}}}\frac{M_{\text{fast}}^{\text{donor}}(t)}{M_{\text{fast}}(t)}, \quad \chi_{\text{slow, norm}}(t) = \frac{1}{\chi_{\text{DP1}}}\frac{M_{\text{slow}}^{\text{donor}}(t)}{M_{\text{slow}}(t)}. \tag{14}$$

The normalised chimerism in the fast and slow populations combined is

$$\chi_{\text{M, norm}}(t) = \chi_{\text{fast, norm}}(t)\frac{M_{\text{fast}}(t)}{M(t)} + \chi_{\text{slow, norm}}(t)\frac{M_{\text{slow}}(t)}{M(t)}. \tag{15}$$

We dealt with different ages at BMT using the same approach as described for the simplest model. We determined

the initial sizes of the subsets $M_{\text{fast}}(t_0)$ and $M_{\text{slow}}(t_0)$ by assuming that fast cells were close to steady state being in quasi-equilibrium with either source, which are changing slowly (Fig. 1B), and allowing $M_{\text{slow}}(t_0)$ to be free. Allowing both population sizes to be free yielded very similar results at the cost of an additional parameter. The numbers of host-derived cells in the fast and slow memory subsets at each time T were then generated from $M_{\text{fast}}(t_0)$ and $M_{\text{slow}}(t_0)$ by running the model forward in time from age t_0 using eqns. 12. The two-phase model is then characterised by five unknowns; $M_{\text{slow}}(t_0)$, the loss rates λ_{fast} and λ_{slow}, the transition rate γ, and the force of recruitment φ. To estimate these parameters we fitted the solutions of eqns. 11, 12, and 15 simultaneously to the timecourses of total memory cell numbers $M(t)$ and the normalised chimerism $\chi_{\text{M, norm}}(t)$, using the empirical forms of $S(t)$ and $\chi_{\text{source, norm}}(\tau)$ where t is host age and τ is time post-BMT. To visualise the fits to data from the clean facility we partitioned the mice into four groups based on age at BMT, and plotted the model predictions for the median age at BMT within each group (Fig. 3B).

The age-dependent loss model

In this model (Fig. 2C) the loss rate λ is a function of the time since entry of a cell or its ancestor into memory, which we denote its age a. The time evolution of the population density of memory cells of age a at host age t is given by

$$\frac{\partial M(t,a)}{\partial t} + \frac{\partial M(t,a)}{\partial a} = -\lambda(a) M(t,a), \tag{16}$$

where the population density of cells of age zero is the rate at which cells flow into memory from the source,

$$M(t, a = 0) = \varphi S(t), \tag{17}$$

and we must specify the overall population density with respect to cell age $M(t_0, a) = g(a)$ at some initial mouse age, t_0. As described above, we assumed all cells present at t_0 are host-derived, and we model their age distribution as $g(a) = \varphi S(t_0)\, e^{pa}$. The free parameter p could be positive or negative, such that older cells can initially be over- or under-represented compared to younger cells. This definition ensures $g(0)$ is the rate of influx of cells of age zero from the source at time t_0, $\varphi S(t_0)$. We explored exponential ($\lambda(a) = \lambda_0\, e^{-a/A}$) and sigmoid ($\lambda(a) = \lambda_0/(1 + (a/A)^n)$) forms for the dependence of the net loss rate λ on cell age, with n = 1, 2, 3, 5 and 10. We found that $n = 3$ consistently yielded the best fits, with the exponential performing the most poorly.

Solving this system using the method of characteristics allows us to track the fates of three cell populations – the host-derived population that was present at t_0, $M^{\text{init}}_{\text{host}}(t,a)$, host-derived cells that entered the population after t_0 $M^{\text{new}}_{\text{host}}(t,a)$, and the donor population $M_{\text{donor}}(t,a)$, all of which entered memory after t_0. Total memory cell numbers at $t \geq t_0$ are then

$$M_{\text{total}}(t) = \int_{a=0}^{t} \left(M^{\text{init}}_{\text{host}}(t,a) + M^{\text{new}}_{\text{host}}(t,a) + M_{\text{donor}}(t,a) \right)\, da. \tag{18}$$

The terms in this expression evolve according to

$$\begin{aligned} M^{\text{init}}_{\text{host}}(t,a) &= g(a - (t - t_0)) \exp\left(- \int_{a-(t-t_0)}^{a} \lambda(s)\, ds \right),\ t - t_0 \leq a \leq t \\ M^{\text{new}}_{\text{host}}(t,a) &= \varphi S_{\text{host}}(t-a) \exp\left(- \int_{0}^{a} \lambda(s)\, ds \right),\ 0 \leq a \leq t - t_0 \\ M_{\text{donor}}(t,a) &= \varphi S_{\text{donor}}(t-a) \exp\left(- \int_{0}^{a} \lambda(s)\, ds \right),\ 0 \leq a \leq t - t_0. \end{aligned} \tag{19}$$

where $S_{\text{host}}(t) = (1 - \chi_{\text{source}}(t))S(t)$ and $S_{\text{donor}}(t) = \chi_{\text{source}}(t)S(t)$. This gives

$$M_{\text{total}}(t) = \int_{a=t-t_0}^{t} g(a-(t-t_0)) \exp\left(-\int_{a-(t-t_0)}^{a} \lambda(s)\, ds\right) da + \varphi \int_{a=0}^{t-t_0} S(t-a) \exp\left(-\int_0^a \lambda(s)\, ds\right) da. \tag{20}$$

The normalised donor chimerism is

$$\begin{aligned} \chi_{\text{M, norm}}(t) = \frac{M_{\text{donor}}(t)}{\chi_{\text{DP1}}\, M_{\text{total}}(t)} &= \frac{\int_{a=0}^{t-t_0} M_{\text{donor}}(t,a)\, da}{\chi_{\text{DP1}}\, M_{\text{total}}(t)} \\ &= \frac{\varphi}{M_{\text{total}}(t)} \int_{a=0}^{t-t_0} \chi_{\text{source, norm}}(t-a) S(t-a) \exp\left(-\int_0^a \lambda(s)\, ds\right) da. \end{aligned} \tag{21}$$

We fit eqns. 20 and 21 to the timecourses of their observed counterparts from host age t_0 onwards. This model has four free parameters; p and φ, which, together with the observed value of $S(t_0)$, specify the initial age distribution of host cells, $g(a) = \varphi S(t_0) e^{pa}$; and λ_0 and A, which specify the form of $\lambda(a)$. The parameters p and φ then determine the initial number of host-derived memory cells;

$$M_{\text{total}}(t_0) \equiv \int_0^{t_0} g(a) da = \varphi S(t_0)(e^{pt_0} - 1)/p. \tag{22}$$

As described above, this model can be fitted simultaneously to data from mice who underwent BMT at different ages, replacing t_0 in eqn. 21 with the age at BMT plus 26d or 28d for clean and dirty mice respectively.

Resistant memory model

In this model, proposed in Gossel *et al.* (2017), the CD4 T_{CM} and T_{EM} populations are assumed to be heterogeneous, each consisting of a 'displaceable' subset turning over at rate λ and continuously supplemented from the source, and an 'incumbent' subpopulation of host cells, $I_{\text{host}}(t)$; these are assumed to be established early in life, not supplemented thereafter, and have a distinct net loss rate λ_I:

$$\begin{aligned} \frac{dM_{\text{donor}}(t)}{dt} &= \varphi \chi_{\text{source}}(t) S(t) - \lambda M_{\text{donor}}(t) && \text{(displaceable, donor)} \\ \frac{dM_{\text{host}}(t)}{dt} &= \varphi(1 - \chi_{\text{source}}(t)) S(t) - \lambda M_{\text{host}}(t) && \text{(displaceable, host)} \\ \frac{dI_{\text{host}}(t)}{dt} &= -\lambda_I I_{\text{host}}(t). && \text{(Incumbent/resistant cells, host)} \end{aligned} \tag{23}$$

All donor-derived cells are assumed to be displaceable and obey the same kinetics as displaceable host-derived cells. We solved eqns. 23 to obtain total memory cell numbers $M_{\text{total}}(t) = M_{\text{donor}}(t) + M_{\text{host}}(t) + I_{\text{host}}(t)$, and the normalised chimerism in memory,

$$\chi_{\text{M, norm}}(t) = \frac{1}{\chi_{\text{DP1}}} \frac{M_{\text{donor}}(t)}{M_{\text{total}}(t)}. \tag{24}$$

For simplicity we assumed that resistant memory cells were stable in number, $\lambda_I = 0$. The incumbent model then has four free parameters ($M_{\text{total}}(t_0)$, $I_{\text{host}}(t_0)$, φ, λ). Multiple ages at BMT were handled as described for the simplest model.

Model selection

We used the corrected Akaike Information Criterion (AICc) to assess the relative support for competing models (Akaike, 1974, Burnham and Anderson, 2002). For a model with K free parameters estimated by maximising the likelihood $\mathcal{L}$ of N observations,

$$\text{AICc} = -2\log(\mathcal{L}) + 2K + \frac{2K(K+1)}{N-K-1}. \tag{25}$$

AICc differences between models of 10 or more are considered highly significant, with most support for the model with the lowest AICc value. We calculated the AICc using the joint likelihood for each model fitted to data from both facilities; therefore K was double the number of parameters in the each model, and $N = 2 \times$ the number of mice in the clean facility + $2 \times$ the number in the dirty facility; the factor 2 appears because each animal yielded the paired measurements of total numbers and donor chimerism of memory T cells.

Acknowledgments

This work was supported by the NIH (R01 AI093870) and the Medical Research Council (MC-PC-13055). We would like to thank Fiona Powrie and the Oxford Centre for Microbiome Studies for germ free mice.

References

Akaike H (1974). A new look at the statistical model identification. *IEEE Transactions on Automatic Control* 19(6):716–723

Beura LK, Hamilton SE, Bi K, *et al.* (2016). Normalizing the environment recapitulates adult human immune traits in laboratory mice. *Nature* 532(7600):512–6

Burnham KP, Anderson DR (2002). *Model Selection and Multimodel Inference*. Springer, second edition

Farber DL (2000). T cell memory: heterogeneity and mechanisms. *Clinical Immunology* 95(3):173–181

Ganusov VV, Borghans JAM, De Boer RJ (2010). Explicit kinetic heterogeneity: mathematical models for interpretation of deuterium labeling of heterogeneous cell populations. *PLoS Comput Biol* 6(2):e1000666

Gossel G, Hogan T, Cownden D, Seddon B, Yates AJ (2017). Memory CD4 T cell subsets are kinetically heterogeneous and replenished from naive T cells at high levels. *Elife* 6:e23013

Gourley TS, Wherry EJ, Masopust D, Ahmed R (2004). Generation and maintenance of immunological memory. In *Seminars in Immunology*, volume 16(5), pages 323–333. Elsevier

Hogan T, Gossel G, Yates AJ, Seddon B (2015a). Temporal fate mapping reveals age-linked heterogeneity in naive T lymphocytes in mice. *Proceedings of the National Academy of Sciences* 112(50):E6917–E6926

Hogan T, Gossel G, Yates AJ, Seddon B (2015b). Temporal fate mapping reveals age-linked heterogeneity in naive T lymphocytes in mice. *Proc Natl Acad Sci U S A* 112(50):E6917–26

Hogan T, Yates A, Seddon B (2017a). Analysing temporal dynamics of T cell division *in vivo* using Ki67 and BrdU co-labelling by flow cytometry. *Bio-protocol* 7(24)

Hogan T, Yates A, Seddon B (2017b). Generation of Busulfan chimeric mice for the analysis of T cell population dynamics. *Bio-protocol* 4(24)

Jameson SC, Masopust D (2009). Diversity in T cell memory: an embarrassment of riches. *Immunity* 31(6):859–871

Jameson SC, Masopust D (2018). Understanding Subset Diversity in T Cell Memory. *Immunity* 48(2):214–226

Kaech SM, Wherry EJ (2007). Heterogeneity and cell-fate decisions in effector and memory CD8+ T cell differentiation during viral infection. *Immunity* 27(3):393–405

Kawabe T, Jankovic D, Kawabe S, *et al.* (2017). Memory-phenotype CD4+ T cells spontaneously generated under steady state conditions exert innate Th1-like effector function. *Science Immunology* 2(12)

Kotani M, Hirata K, Ogawa S, *et al.* (2006). CD28-dependent differentiation into the effector/memory phenotype is essential for induction of arthritis in interleukin-1 receptor antagonist-deficient mice. *Arthritis & Rheumatism* 54(2):473–481

Lee YJ, Jameson SC, Hogquist KA (2011). Alternative memory in the CD8 T cell lineage. *Trends in Immunology* 32(2):50–56

Mandl JN, Monteiro JP, Vrisekoop N, Germain RN (2013). T cell-positive selection uses self-ligand binding strength to optimize repertoire recognition of foreign antigens. *Immunity* 38(2):263–274

Min B, McHugh R, Sempowski GD, *et al.* (2003). Neonates support lymphopenia-induced proliferation. *Immunity* 18(1):131–140

Min B, Paul WE (2005). Endogenous proliferation: burst-like CD4 T cell proliferation in lymphopenic settings. In *Seminars in Immunology*, volume 17(3), pages 201–207. Elsevier

Moussion C, Girard JP (2011). Dendritic cells control lymphocyte entry to lymph nodes through high endothelial venules. *Nature* 479(7374):542–546

Rane S, Hogan T, Seddon B, Yates AJ (2018). Age is not just a number: Naive T cells increase their ability to persist in the circulation over time. *PLoS Biol* 16(4):e2003949

Seddon B, Tomlinson P, Zamoyska R (2003). Interleukin 7 and T cell receptor signals regulate homeostasis of CD4 memory cells. *Nature Immunology* 4(7):680–686

Sprent J, Surh CD (2011). Normal T cell homeostasis: the conversion of naive cells into memory-phenotype cells. *Nature Immunology* 12(6):478

Vezys V, Yates A, Casey KA, *et al.* (2009). Memory CD8 T-cell compartment grows in size with immunological experience. *Nature* 457(7226):196–9

Webb LV, Barbarulo A, Huysentruyt J, *et al.* (2019). Survival of Single Positive Thymocytes Depends upon Developmental Control of RIPK1 Kinase Signaling by the IKK Complex Independent of NF-κB. *Immunity* 50(2):348–361.e4

Wendland M, Willenzon S, Kocks J, *et al.* (2011). Lymph node T cell homeostasis relies on steady state homing of dendritic cells. *Immunity* 35(6):945–957

Younes SA, Punkosdy G, Caucheteux S, *et al.* (2011). Memory phenotype CD4 T cells undergoing rapid, nonburst-like, cytokine-driven proliferation can be distinguished from antigen-experienced memory cells. *PLoS biology* 9(10):e1001171

Zhang Z, Li J, Zheng W, *et al.* (2016). Peripheral Lymphoid Volume Expansion and Maintenance Are Controlled by Gut Microbiota via RALDH+ Dendritic Cells. *Immunity* 44(2):330–342

Supporting Information

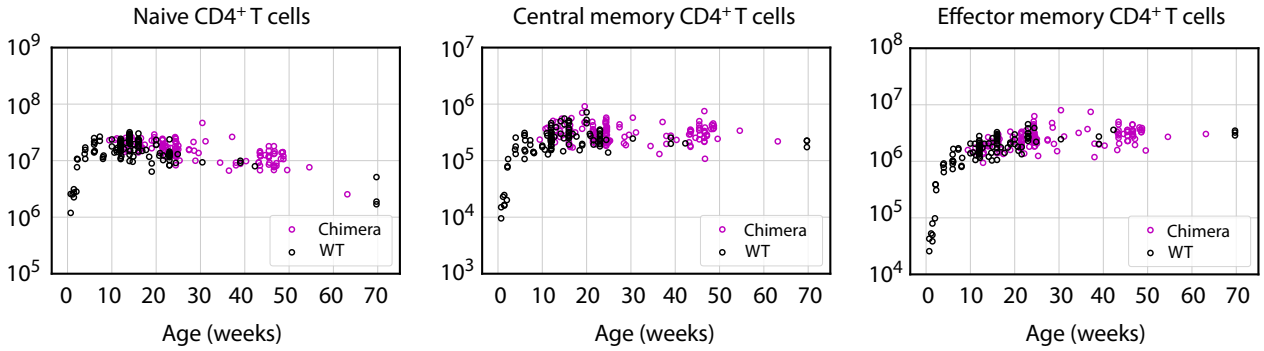

Figure S1: **Busulfan chimeric mice exhibit normal numbers of CD4 naive, T_{CM} and T_{EM} cells.**

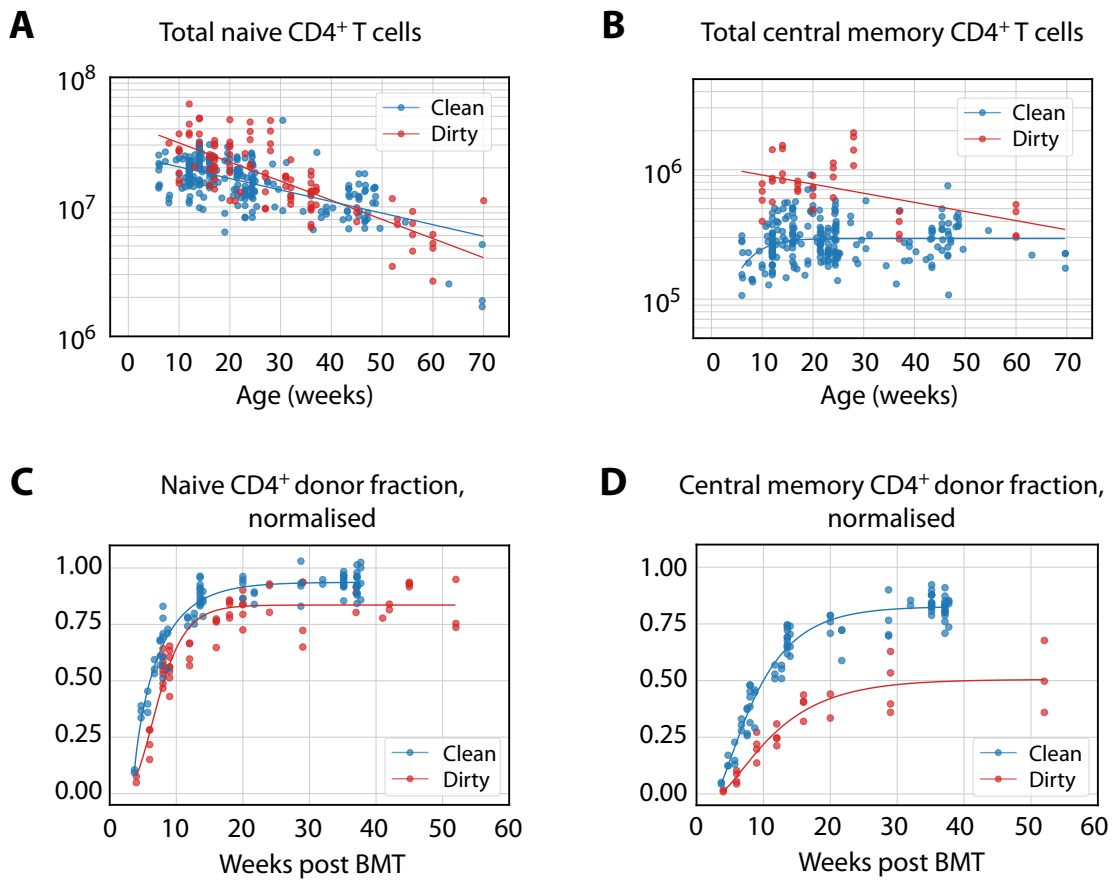

Figure S2: **Empirical descriptions of the size and chimerism of the putative source populations for T_{CM} and T_{EM} in adult mice.** Naive T cell numbers, and memory cell numbers in dirty mice, were modeled with exponential decay ($S(t) = S_{\max}e^{-rt}$); memory cell numbers in clean mice were described with $S(t) = S_{\max}/(1 + e^{-rt}(S_{\max} - S_{\min})/S_{\min})$. Donor fraction (normalised chimerism) curves were described with the generalised logistic function $\chi(t) = 1/(A + Be^{-rt})^{1/c}$ using the pooled data from mice at multiple ages post-BMT; curves specific to different ages at BMT were very similar.

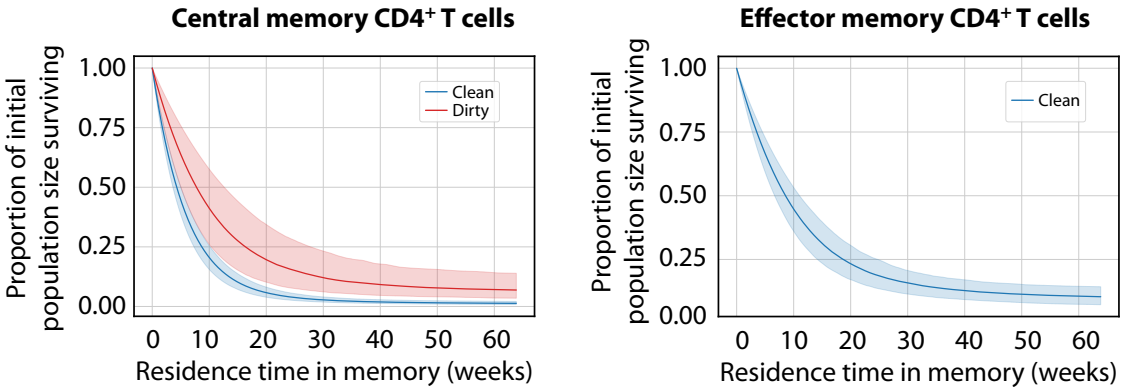

Figure S3: **Predicted survival curves for populations entering memory using the age-dependent loss model**. These curves reflect the net loss rate $\lambda(a)$, which is the balance of loss and self-renewal; therefore, the curves reflect the persistence of a self-renewing population with time since it entered memory, rather than the survival of individual cells. For T_{EM} in dirty mice, $\lambda(a)$ was close to zero implying no loss of populations within memory.